

Image Analysis and Interactive Visualization Techniques for Electron Microscopy Tomograms

Lennart Svensson

*Faculty of Forest Sciences,
Centre for Image Analysis,
Uppsala*

Doctoral Thesis
Swedish University of Agricultural Sciences
Uppsala 2014

Acta Universitatis agriculturae Sueciae
2014:94

ISSN, 1652-6880
ISBN (print version), 978-91-576-8136-2
ISBN (electronic version), 978-91-576-8137-9
©2014 Lennart Svensson, Uppsala
Print: SLU Service/Repro, Uppsala 2014

Image Analysis and Interactive Visualization Techniques for Electron Microscopy Tomograms

Abstract

Images are an important data source in modern science and engineering. A continued challenge is to perform measurements on and extract useful information from the image data, i.e., to perform image analysis. Additionally, the image analysis results need to be visualized for best comprehension and to enable correct assessments. In this thesis, research is presented about digital image analysis and three-dimensional (3-D) visualization techniques for use with transmission electron microscopy (TEM) image data and in particular electron tomography, which provides 3-D reconstructions of the nano-structures.

The electron tomograms are difficult to interpret because of, e.g., low signal-to-noise ratio, artefacts that stem from sample preparation and insufficient reconstruction information. Analysis is often performed by visual inspection or by registration, i.e., fitting, of molecular models to the image data. Setting up a visualization can however be tedious, and there may be large intra- and inter-user variation in how visualization parameters are set. Therefore, one topic studied in this thesis concerns automatic setup of the transfer function used in direct volume rendering of these tomograms. Results indicate that histogram and gradient based measures are useful in producing automatic and coherent visualizations.

Furthermore, research has been conducted concerning registration of templates built using molecular models. Explorative visualization techniques are presented that can provide means of visualizing and navigating model parameter spaces. This gives a new type of visualization feedback to the biologist interpreting the TEM data. The introduced probabilistic template has an improved coverage of the molecular flexibility, by incorporating several conformations into a static model. Evaluation by cross-validation shows that the probabilistic template gives a higher correlation response than using a Protein Databank (PDB) devised model. The software ProViz (for Protein Visualization) is also introduced, where selected developed techniques have been incorporated and are demonstrated in practice.

Keywords: interdisciplinary image analysis and visualization, electron tomography, interactive software tools

Author's address: Lennart Svensson, SLU, Centre for Image Analysis, Box 337, SE-751 05 Uppsala, Sweden.

E-mail: lennart.svensson@slu.se

Contents

List of Publications	7
List of Abbreviations	9
1 Introduction	11
1.1 Project background	13
1.2 Scope and outline	14
2 Digital image analysis	15
2.1 Image acquisition	15
2.2 Image representation and pixel relationships	16
2.3 Basic operations and transformations	17
2.4 Pre-processing	19
2.5 Identification	23
3 Transmission electron microscopy	27
3.1 Brief history	27
3.2 Electron microscope	28
3.3 Electron tomography	30
4 Volume visualization and interaction	35
4.1 Ray casting DVR	36
4.2 Transfer functions and automatic visualization	38
4.3 Stereoscopic visualization and volume interaction	39
5 Contributions	41
5.1 Paper I	41
5.2 Paper II	43
5.3 Paper III	44
5.4 Paper IV	45
5.5 Paper V	46
6 Summary and discussion	49
7 Current development and challenges	51
8 Svensk sammanfattning	53

The contribution of Lennart Svensson to the papers included in this thesis was as follows:

- I Main parts of idea, implementation, experiments and writing.
- II Part of idea. Main parts of implementation, experiments and writing.
- III Main parts of idea, implementation, experiments and writing.
- IV Main parts of idea, implementation, experiments and writing.
- V Part of idea. Main contributor to implementation. Main parts of experiments and writing.

List of Publications

This thesis is based on the work contained in the following papers, referred to by Roman numerals in the text:

- I Lennart Svensson, Ingela Nyström, Stina Svensson, Ida-Maria Sintorn (2011). Investigating measures for transfer function generation for visualization of MET biomedical data. *In Proceedings of the WSCG Conference of Computer Graphics 2011*, pp. 113–120.
- II Lennart Svensson, Anders Brun, Ingela Nyström, Ida-Maria Sintorn (2011). Registration parameter spaces for molecular electron tomography images. *In Proceedings of the International Conference on Image Analysis and Processing (ICIAP)*, Lecture Notes in Computer Science 6978, pp. 403–412.
- III Lennart Svensson, Johan Nysjö, Anders Brun, Ingela Nyström, Ida-Maria Sintorn (2012). Rigid template registration in MET images using CUDA. *In Proceedings of the International Conference on Computer Vision Theory and Applications (VISAPP)*, SciTePress, pp. 418–422.
- IV Lennart Svensson, Ida-Maria Sintorn (2013). A probabilistic template model for finding macromolecules in MET volume images. *In Proceedings of the 6th Iberian Conference on Pattern Recognition and Image Analysis (IbPRIA)*, Lecture Notes in Computer Science 7887, pp 855–862.
- V Lennart Svensson, Stina Svensson, Ingela Nyström, Fredrik Nysjö, Johan Nysjö, Aurelie Laloëuf, Lianne den Hollander, Anders Brun, Sergej Masish, Ida-Maria Sintorn. ProViz: a tool for explorative 3-D visualization and template matching in electron tomograms. *Submitted for journal publication*, 2014.

List of Abbreviations

ART	Algebraic Reconstruction Technique
CC	Cross-Correlation
CCD	Charge-Coupled Device
COMET	Constrained Maximum Entropy Tomography
CPU	Central Processing Unit
FBP	Filtered Back Projection
GPU	Graphics Processing Unit
NCC	Normalized Cross-Correlation
PDB	Protein Data Bank
RCC	Requested Connected Components
SIRT	Simultaneous Iterative Reconstruction Technique
TEM	Transmission Electron Microscopy

1 Introduction

Digital image analysis is the extraction of relevant information from digital images. It has increased in importance due to the digitization in society and become part of technologies used in everyday life. It is used, e.g., in cell phones to recognize faces for focusing the digital camera and for scanning QR and bar codes. The objective of image analysis is often to find the number and location of certain objects or entities in images and characterize their properties. Image analysis is often performed in conjunction with data visualization to present both the image data and the analysis results. In this thesis, image analysis is applied to transmission electron microscopy (TEM) images of biological material. The primary question addressed is how existing visualization and matching methods used in TEM can be improved, in particular for use in an interactive setting.

TEM is capable of depicting biological material with a resolution in the nanometer range. At this resolution, it is possible to perform studies at sub-cellular level, which is a valuable source of knowledge for the biological sciences. In some cases, individual macro-molecules can also be identified, e.g., the large protein RNA polymerase. At the microscope, the obtained images

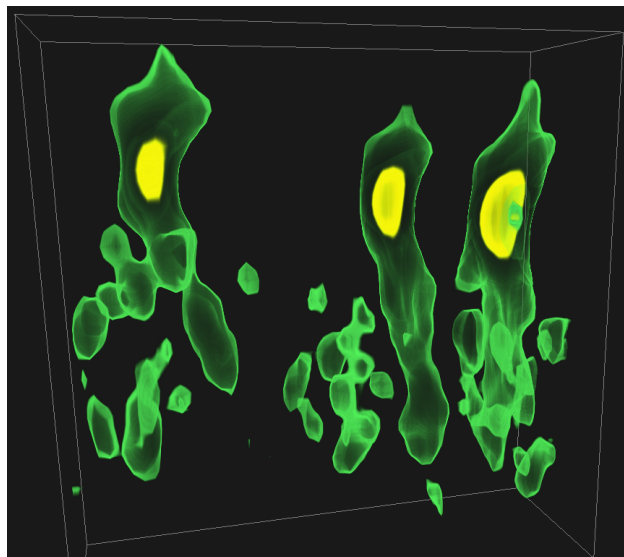


Figure 1: A visualization of a volume image from electron tomography, showing so called fiducial, i.e. reference, gold particles (yellow) that are used to mark cellular structures (green) through antibody chains (also green). Tomogram data courtesy of Aurelie Laloef, Karolinska Institutet.

are two-dimensional (2-D) projections of the studied sample. With multiple images of the sample, taken at different angles, it is possible to create a three-dimensional (3-D) reconstruction, a *tomogram*. An example tomogram visualization is shown in Figure 1. The technique for acquiring this kind of data is called *electron tomography*. The 3-D reconstruction is usually represented in a *volume image*, which can be seen as a 3-D grid sampling of a continuous 3-D field. The volume images from electron tomography can show the particular 3-D shape that different molecules have *in situ*, i.e., in the sample. In principle, the images can also show how the molecules bind to other molecules [36]. Increased knowledge about the structural behavior of proteins, as well as of other biological compounds, can eventually contribute to the development of new medical treatments.

However, performing a TEM study requires significant efforts and the results are not always clear. Sample preparation, measurements and data analysis are both labor intensive and time demanding, and the procedures are highly sensitive to deviations in settings and physical environment. For in-situ tomography studies, the biologists interest is often to locate certain proteins in the image data. The interpretation of TEM images is however difficult, because of, e.g., high noise levels and image artefacts. The data is often analyzed i) by visual inspection, ii) by segmentation of components using image analysis and iii) by matching templates and molecular models in the data. In this thesis, research is presented about possible improvements in these areas. Questions that have come into focus during the work, and been used for guidance are:

- can the setup of the visualization of the volume images from electron tomography be partially automatized?
- how can the data volumes and matching results be visualized for better comprehension?
- how much can the time performance of the matching routines be enhanced using graphics processing unit (GPU) parallelization?
- is it possible to increase the matching detection rates by creating volume templates differently?
- how should a software be designed to make best use of the developed techniques, and complement existing software for user-friendly interactive analysis?

is it possible within this work to create software that provides functionality not currently available in other TEM software tools?

To address these questions, TEM data analysis is here mainly approached from an image analysis point of view, and combined with adaptations of 3-D visualization techniques. As mentioned above, image analysis is often performed to find objects or constituent parts in an image, and to characterize the properties of these. The analysis is based on the similarities and dissimilarities of the appearance of these objects. It is a general framework that can be adapted to all kinds of image data, from telescope images in astronomy to the nanoscale images in TEM. Another analysis approach in TEM, very widely used, is what might be called a data source analysis approach. In this approach, molecular models are matched into the TEM image volumes. Recently, techniques of this kind has also been included in the 3-D reconstruction process [19]. In image analysis, the characteristics of the objects in the images are often directly used for designing models and algorithms, whereas the latter approach centers on using molecular information from different sources as well as from molecular simulation. The approaches are also overlapping and the techniques presented in this thesis reside in that overlap to a high extent.

3-D TEM data is lacking many of the features often used in image analysis (e.g. color and texture) that can separate structures of interest from other material. The most significant cues in TEM image data are the 3-D shapes and the spatial arrangement of potential proteins. Analysis of TEM volumes is often performed using volume image correlation with different correlation metrics [49]. In image analysis, this process is categorized as *template matching*. Template matching can sometimes also denote the fitting of deformable models [8], but here it is used only in the meaning of fitting one template image in a larger image. The questions addressed in this thesis centers on correlation matching, using template matching as base method.

1.1 Project background

The research behind this thesis has been carried out primarily within the ProViz (Protein Visualization) project. The project has been a collaboration between the Centre for Image Analysis in Uppsala¹ and the companies Sidec Technologies and SenseGraphics². A requirement of the funding programme that supported the ProViz project was to create a so called *demonstrator* of the accomplished work, for demonstrating the practical value and use of the research. In the beginning of the project, Sidec Technologies left the project due to external factors, and collaboration was instead initiated

¹<http://www.cb.uu.se/>

²<http://www.sensegraphics.com/>

with the Department of Cell and Molecular Biology at the Karolinska Institute in Stockholm³.

1.2 Scope and outline

In this thesis, one aspect of automating the visualization setup for 3-D TEM images is investigated (Paper I), ways to improve interactive tools are suggested (Papers II, III and V), and soft templates created by averaging is explored (Paper IV). More specifically, the papers have the following content.

- In Paper I, the question about automatic visualization is addressed. The results point in the direction that the ordinary graylevel histogram and possibly a gradient based measure would be most suitable for this purpose.
- In Paper II, scoring volumes are presented and tested in the context of biological TEM. Scoring volumes are 3-D visualizations of the correlation results in the parameter space domain. They are explored in the context of analyzing correlation results from template matching.
- In Paper III, GPU acceleration techniques for template matching are presented and compared.
- In Paper IV, a method for building templates that models protein flexibility is introduced.
- In Paper V, the ProViz software tool for visualization, template correlation and particle removal (dust removal) is described and demonstrated. The software incorporates techniques from Papers II and III, and is influenced by the other papers.

The topics of the thesis have been selected because considered to be:

- i) interesting research questions,
- ii) relevant for our collaborators and other biological researchers,
- iii) within the original research plan for the ProViz research grant.

The next three chapters give an overview of the research areas and terminology relevant for the papers. In Chapter 5, the contributions of the papers are summarized. In Chapters 6 and 7, a discussion about the results and possible future research topics follows.

³<http://ki.se/en/cmb/>

2 Digital image analysis

Images are 2-D or 3-D signals with one or several channels (e.g., grayscale intensity or color). *Image analysis* is about extracting and processing useful information from images, whereas digital image analysis is about performing this using computers. This often requires elaborate algorithms and high computational power, but presents great opportunities, e.g., for automation and for performing exact measurements.

Digital image analysis typically follows a few general steps. The first step is *image acquisition*, in which sensor measurements are transformed into a representation of an image, which is often a square grid of sampled intensities. These intensities, the "picture elements", are denoted *pixels* and, for 3-D images, the "volume elements" are denoted *voxels*. Each pixel or voxel represents one scalar intensity (for grayscale images) or vector (e.g., for color). After acquisition, the next step is usually *pre-processing*, to enhance features of interest, to suppress noise and to perform data normalization, normally by scaling the intensity distribution into a standard range. The process can continue with *segmentation*, which partitions an image into regions representing constituent parts, e.g., objects, using the notion that regions with similar properties often represent the same class of objects or material. During segmentation, the borders between segmented regions are determined, which is denoted *delineation*. Next, *classification* or *recognition* of the regions is performed. After these steps, objects have been identified in the image. During this process or afterwards, template models may be fitting to the objects, which is often denoted *registration*. The process may continue with *post-processing*, such as measurements of object properties or object visualizations. This bottom-up approach is common for image analysis tasks, with first processing an image locally to enhance *features*, i.e., local characteristics of the image, and then continuing the analysis on a higher level. In this chapter, concepts relevant for the papers included in this thesis will be described. For detailed descriptions of all the processing steps stated above, the reader is referred to an image analysis textbook [18].

2.1 Image acquisition

The digital images that are analyzed can be obtained using different *imaging modalities*, e.g., digital cameras, medical imaging devices (MRI, X-ray, PET etc.) or electron microscopes. To form the images an information channel is needed, which conveys the information from what is depicted to the measuring sensor, e.g., the image sensor in a digital camera. Electromagnetic waves is the most common information channel, with different bands

of the spectrum (infra-red light, normal light, ultra-violet light, X-ray, etc.) suitable for different applications. Another information channel is sound waves, e.g., used in ultrasound imaging. For electron microscopes, a ray of accelerated electrons is the information bearing medium.

The signal is detected by the sensor, which often is an integrated circuit that is using the photoelectric effect to detect electromagnetic waves of shorter wavelength. These circuits are also commonly used in electron microscopes as the electrons are first converted to photons using a phosphorous screen. In this setup, the analog electrical signal is digitized to form a 2-D digital image. There are also imaging modalities that rely on computational post-processing to create the obtained image. This is commonly the case for 3-D imaging.

The sensor detects the signal, which already can be in image format (e.g., in a digital camera) or measure point or line data that needs to be further processed to form the image (e.g., in a desktop scanner).

2.2 Image representation and pixel relationships

A continuous image is a function

$$I_c : \mathbb{R}^n \rightarrow \mathbb{R}^k \quad (1)$$

where \mathbb{R} is the set of real numbers, n is the dimension of the image coordinate space, which is often either 2-D or 3-D, and k is the dimension of the output. When an image is stored and processed in a computer as a digital image, it is discretized. This digital image can be expressed as a function

$$I_d : \mathbb{Z}^n \rightarrow \mathbb{R}^k \quad (2)$$

where \mathbb{Z} is the set of integers. The output is however restricted by the available numeric precision, which is not included in this expression. In words, an image is a mapping between vector coordinates, e.g., (x, y, z) , defining the location of a pixel in a grid, and the image function output at these coordinates, e.g., a color vector (r, g, b) . If the image is a grayscale image, the function output is scalar, and the image is a *scalar field*. Alternatively, if the output is a vector, e.g., for a color image, the image is a *vector field*. Images in 3-D are called volume images, or just volumes.

The pixels adjacent to a pixel are called neighbors to that pixel. Vertical and horizontal neighbors form the *4-neighborhood* set for a pixel, and also including the diagonal neighbors gives the *8-neighborhood* [18]. The neighbors in a 4-neighborhood are called *4-adjacent* to the center pixel, and the neighbors in the 8-neighborhood are called *8-adjacent*. In 3-D, it is common

to use 6-, 18- and 26-adjacencies and corresponding neighborhoods. These are created in a similar way as in 2-D. A *local region* is a more general term for the set of pixel near a center point, either in the form of a neighborhood as stated above or a pixel set further extended from the center.

The *path* between two pixels is any sequence of adjacent pixels that connects the two pixels. Hence, there are also 4- and 8-paths. Two pixels are *connected* with respect to a set of pixels S if there is a path between them consisting only of pixels in the set S . A set of pixels where all pixels are connected creates a *connected component*.

Two common measures for distances in digital images are the *city block distance* and the *Euclidean distance*. The city block distance between two pixels is the sum of the vertical and horizontal distance, i.e., the sum of the absolute values of the coordinate difference in x and y . The Euclidean distance corresponds to the length of a straight line connecting the pixels, i.e.,

$$D_e(p, q) = ((x - s)^2 + (y - t)^2)^{1/2}, \quad (3)$$

where p and q are pixels with coordinates (x, y) and (s, t) , respectively.

2.3 Basic operations and transformations

Interpolation is used to calculate image intensities for coordinates in between of points in the sampling grid. *Nearest neighbor interpolation* uses the graylevel intensity from the nearest sampling point in the grid directly, but for more accurate estimation, a polynomial can be fitted to the grid intensities. Using a first-degree polynomial results in *linear interpolation*, a second-degree in *quadratic interpolation* and a third-degree in *cubic interpolation*.

Intensity thresholding divides an image into two sets, depending if the intensity is above or below a threshold value. It is generally performed as a per pixel base operation, that leaves all intensities above or equal to the threshold unchanged, and sets the rest of the pixel values to, e.g., zero. However, if the exact contour of the thresholded region is of importance, it can be better to delineate an interpolated field of the image. When visualizing electron tomograms, often only intensities above a threshold are visualized, which means that a kind of thresholding is performed implicitly, without altering the underlying data.

The *intensity histogram* of an image shows the distribution of intensities. Objects of one class might cover a similar range of intensities, and multiple objects of this class can form a distribution that may be seen in the intensity histogram. Multiple objects of different classes may form distinguishable

distributions in the histogram. In these cases, a histogram analysis might give an appropriate threshold or aid in identification of the objects in the image. Other image characteristics can also be measured over the intensity range.

Frequency domain representation created by Fourier transformation is essential in image analysis. It can be used in all steps of images analysis, both to enable certain computations and to speed up calculations. The Fourier transformed signal is a convolution/cross correlation between the input function and a complex sinusoid, and the discrete 1-D Fourier transform is defined as

$$F(u) = \sum_{x=0}^{N-1} f(x)e^{-j2\pi ux/N}, \quad (4)$$

where $f(x)$ is the discrete input function, N the number of samples in the input, $F(u)$ the Fourier transformed output function, and u and x the sample indices, over the same range. The Fourier transformation can also be performed in 2-D and 3-D, which are the variants mainly used in image analysis. For these dimensions, it is generally calculated as a 1-D Fourier transformation over each dimension.

Another central image transformation is the calculation of the first and second order derivatives of an image – the *gradient vector* and the *Hessian matrix* of each point in the image. For a grayscale volume image, the gradient field is a vector field where each vector consists of the three partial derivatives:

$$\mathbf{g} = \nabla f = \left(\frac{\partial f}{\partial x}, \frac{\partial f}{\partial y}, \frac{\partial f}{\partial z} \right). \quad (5)$$

An example of a gradient field for a 2-D image is shown in Figure 2. The Hessian is the matrix of second order partial derivatives. For a volume image $f(x, y, z)$ it is

$$\mathbf{H} = \begin{bmatrix} \frac{\partial^2 f}{\partial x^2} & \frac{\partial^2 f}{\partial x \partial y} & \frac{\partial^2 f}{\partial x \partial z} \\ \frac{\partial^2 f}{\partial y \partial x} & \frac{\partial^2 f}{\partial y^2} & \frac{\partial^2 f}{\partial y \partial z} \\ \frac{\partial^2 f}{\partial z \partial x} & \frac{\partial^2 f}{\partial z \partial y} & \frac{\partial^2 f}{\partial z^2} \end{bmatrix}. \quad (6)$$

The Hessian is, e.g., used when calculating the curvature in a volume image.

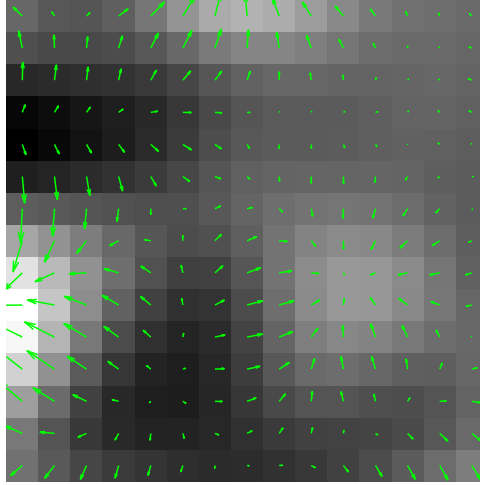


Figure 2: A section of a digital image, interpolated with nearest neighbor interpolation, and the gradient vector field of the image (depicted with arrows).

2.4 Pre-processing

Pre-processing is an image-to-image mapping, i.e., the processing step takes an image as input and generates one or several images as output. The purposes include enhancing the sought information, suppressing noise and unwanted information, and normalizing and transforming the data into a suitable format for subsequent processing steps.

Noise is often predominant at high frequencies in measured data. Therefore, noise removal is often performed by filtering out high frequencies fully or partially. This low-pass filtering is usually performed directly in the *spatial domain*, i.e., the normal image space. It is calculated by convolution or cross-correlation with a filtering function, e.g., a Gaussian function for so called Gaussian filtering as illustrated in Figure 3. In 1-D, a Gaussian function can be expressed as

$$f(x) = \frac{1}{\sigma\sqrt{2\pi}} e^{-(x-\mu)^2/2\sigma^2}, \quad (7)$$

where σ is the standard deviation and μ the average of the distribution the function expresses. A slice of the Gaussian is used when performing this operation with discretized signals. A symmetric 2-D Gaussian is shown in Figure 4. For filtering a 2-D image, the filtering function is also expressed in a 2-D image, which is called *kernel* or *mask* [18]. The cross-correlation is

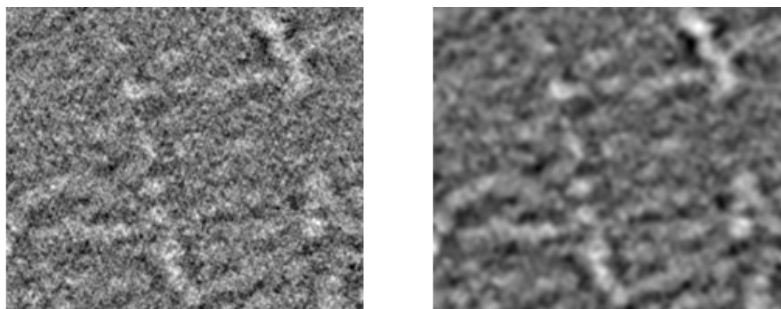


Figure 3: A slice of a 3-D reconstruction before (left) and after (right) Gaussian filtering with a symmetric kernel. This filtering preserves the signal strength at low frequencies and suppresses it at high frequencies, where the noise is predominant.

calculated using

$$g(\mathbf{x}) = \sum_{\mathbf{s} \in \mathcal{R}(\mathbf{x})} k(\mathbf{s})f(\mathbf{x} + \mathbf{s}) \quad (8)$$

where k the kernel, f the input image, g the filtered image and $\mathcal{R}(\mathbf{x})$ the local region of \mathbf{x} . In words, each new sample in the filtered image is a weighted average of the local region, with the kernel coefficients as weights.

The boundaries between different materials or objects in an image are often characterized by a sharp transition in intensity. Therefore, first and second order derivative filters, gradient and Laplacian filters, are used to enhance contours in images.

The gradient can be calculated by convolving the image with the kernels in the upper row in Figure 5. Using these directly will however make the filtering highly sensitive to noise. Applying Gaussian smoothing before calculating the gradient will reduce this effect. These two steps of Gaussian smoothing and gradient kernel convolution can be combined, by convolving with the first partial derivatives of the Gaussian instead, which are shown in the lower row in Figure 5. In 3-D, a third mask is added along the additional dimension for the upper row.

For 3-D structures, a central characteristic is how a surface is curved. This is used in Paper I, and is of general importance for describing 3-D shape. The so called principal curvatures κ_1 and κ_2 measure the maximal and minimal bending of a surface at a particular point. A cylinder, for example, has a high value for κ_1 while κ_2 is zero, since the surface is only curved in

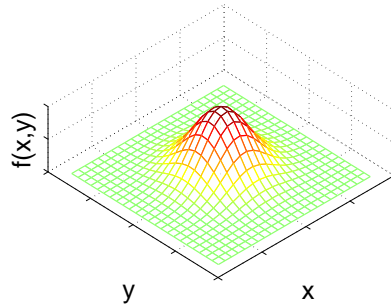


Figure 4: A symmetric 2-D Gaussian distribution, with a characteristic bell shape appearance. This type of function is often used as smoothing kernel, but generally with a coarser sampling, e.g., sampled over a 5×5 image mask. The 2-D Gaussian is composed of 1-D Gaussians along lines intersecting the center point. A symmetric 3-D Gaussian distribution is composed of 1-D Gaussians in a corresponding way.

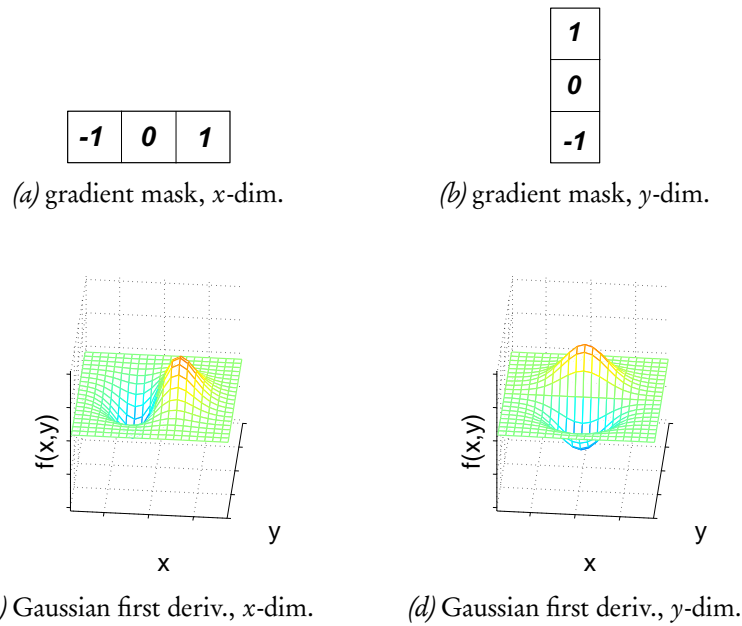


Figure 5: The upper row shows the pixel weights in convolution kernels that can be used for estimating horizontal and vertical gradient components. For increased robustness to noise, Gaussian gradient functions are often used instead. 2-D examples of these are shown on the lower row. The weights in the masks are the highest in a circular area.

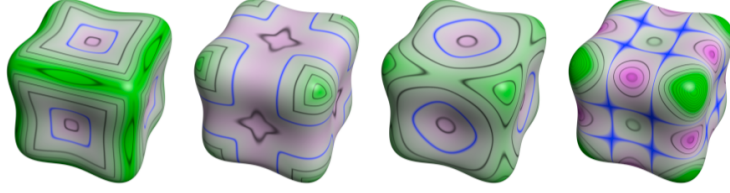


Figure 6: Color coded examples of curvature measures. Left to right: first principal curvature κ_1 showing the maximum curvature, second principal curvature κ_2 showing the minimal curvature, mean curvature $(\kappa_1 + \kappa_2)/2$, and Gaussian curvature $\kappa_1\kappa_2$. Images courtesy of G. Kindlmann [28].

one direction. These measures are often combined into the mean curvature $(\kappa_1 + \kappa_2)/2$ and Gaussian curvature $\kappa_1\kappa_2$. A color coded example from Kindlmann [28] on these curvature measures is shown in Figure 6. The procedure for calculating these, following the same paper, is

1. Calculate the first partial derivatives comprising the gradient \mathbf{g} , compute the normal $\mathbf{n} = -\mathbf{g}/|\mathbf{g}|$, and a matrix $\mathbf{P} = \mathbf{I} - \mathbf{nn}^T$ that projects to the tangent plane of the local iso-surface.
2. Calculate the second order partial derivatives comprising the Hessian \mathbf{H} . Compute $\mathbf{G} = -\mathbf{PHP}/|\mathbf{g}|$.
3. Compute the trace T and Frobenius norm F of \mathbf{G} .
 $\kappa_1 = \frac{1}{2}(T + \sqrt{2F^2 - T^2})$, $\kappa_2 = \frac{1}{2}(T - \sqrt{2F^2 - T^2})$

The trace of a $n \times n$ square matrix A is the sum of the diagonal elements

$$\text{Tr}(A) = \sum_{i=1}^n a_{ii}, \quad (9)$$

the Frobenius norm of an $m \times n$ matrix A is

$$\|A\|_F = \sqrt{\sum_{i=1}^m \sum_{j=1}^n |a_{ij}|^2}. \quad (10)$$

The three smoothed kernels for calculating the second order partial derivatives in 2-D are shown in Figure 7.

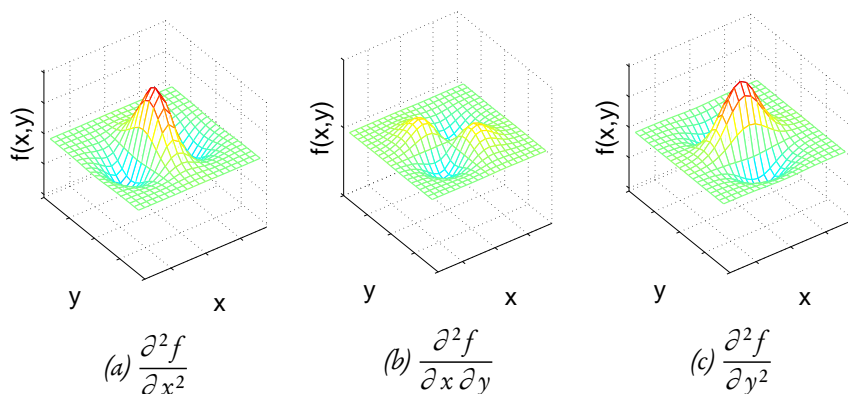


Figure 7: Second order derivatives of a 2-D Gaussian. Corresponding functions for a 3-D Gaussian can be used to calculate the curvature in a 3-D volume.

2.5 Identification

It is possible to determine the structure of many molecules with atomic precision by so called *X-ray crystallography*. In this technique, a crystal structure of one kind of molecule is grown. Exposing the crystal to an X-ray beam results in a diffraction pattern, which can be used to reconstruct the 3-D structure of a single crystal element. The measurement technique builds on the fact that the elements in the crystal have the same spatial structure. The models created by this techniques, the X-ray crystallography structures, can be used to find instances of a molecule in a TEM volume image, by correlating with a template volume image calculated from the determined X-ray structure. Since X-ray crystallography can give molecular reconstructions at an atomic level, this is denoted a *high resolution* structure, whereas TEM images are, in relation to X-ray crystallography, giving *medium* to *low resolution* data. The high-resolution structures from X-ray crystallography are collected in the Protein Database⁴ (PDB).

The static models are cross-correlated with the TEM volumes to find possible locations of a molecule, in a *template matching* procedure. Tools for performing this include Situs by Wriggers [50], CoAn by Volkman [48], DockEM by Roseman [41], EMfit by Rossmann [42] and Foldhunter by Jiang [26]. An overview by Wriggers of different correlation metrics for static template matching in TEM images concluded that cross-correlation using local normalization and cross-correlation with Laplacian pre-processing

⁴<http://pdb.org/>

were the most robust of the studied correlation metrics [49]. The overview by Vasishatan [46] concluded that the Laplacian-based cross-correlation as well as a mutual information based correlation score, were the most promising scores for low resolution data.

However, shape variability is not included in the X-ray structures. An ideal model should capture the degrees of freedom of a modeled object as exactly as possible, i.e., it should capture object variability with as few parameters as possible. Extracting shape variability information for a protein molecule is difficult, since molecules cannot easily be observed for a range of conformations and molecular dynamics are hard to simulate. Molecular dynamics simulations are often restricted to tens or hundred of nanoseconds, which is much shorter than the time periods for many important biological processes [51]. Another issue is accounting for variability in the local environment which the molecule can be found in.

From a modeling point of view, a general strategy for handling molecular flexibility is to fit a model to a TEM volume using shape *regularization*, i.e. penalty for complex or improbable molecule states. Without considering any observations, there are molecule shapes that are more probable to appear, e.g., in low energy states. At a general level, this can be seen as a prior distribution in a Bayesian perspective. More concretely, an often used strategy to model molecular flexibility is to divide a macromolecule into rigid parts which are linked with hinge regions, and where parameters specify maximum bending. This can be, e.g., be performed using QDOCK in Situs. Recently, efforts have been made in incorporating molecular dynamics directly in estimating the prior probability [20][37][45]. Although efforts have been made in this regard, it is debated whether flexible models yet are better to use than the static models [47]. The choice of fitting method depends on many factors, e.g., the resolution and symmetry of the density map, the availability of additional restraints, and the accuracy of component model [52].

In the work presented in this thesis, normalized cross correlation (NCC) is used as the model correlation technique. Static template matching using NCC can be described by:

$$g(\mathbf{x}) = \frac{\sum_{\mathbf{s} \in \mathcal{R}(\mathbf{x})} (f(\mathbf{x} + \mathbf{s}) - \bar{f}_{\mathcal{R}(\mathbf{x})})(k(\mathbf{s}) - \bar{k})}{\sigma_{\mathcal{R}(\mathbf{x})} \sigma_k} \quad (11)$$

with f and k representing the image and the template, and

\mathbf{x}	current point
$\mathcal{R}(\mathbf{x})$	the local region of the current point, i.e., the image region where the template is currently positioned
$\bar{f}_{\mathcal{R}(\mathbf{x})}$	the average of the local neighborhood
$\sigma_{\mathcal{R}(\mathbf{x})}$	the standard deviation of the local neighborhood
\bar{k}	the average of the template
σ_k	the standard deviation of the template

The computation is often performed in the Fourier domain for computational efficiency, and pre-computed sum tables [33] can be used for further optimization.

3 Transmission electron microscopy

TEM is the transmission microscopy technique with the highest resolution (see Figure 8), contributing greatly to the field of structural biology. It enables looking at biological structures *in situ*, i.e., in their natural context in a biological sample, to obtain information about where a protein is located and how it is interacting with the environment. TEM is also used to study *in vitro* samples, i.e., cells or biological molecules studied outside their normal biological context in a solution. The solution can contain many macromolecules of one type, and with the abundance of examples it is possible to extract more information about a molecule's structure and flexibility.

3.1 Brief history

Electron microscopy was pioneered in the 1930s, with Ernst Ruska and Max Knoll as the first to build a working prototype of a transmission electron microscope in 1931. Their progress immediately attracted other researchers to the field, but in the biological sciences the skepticism towards TEM was widespread. The specimens were destroyed by the electron beam and dehydrated because of the vacuum needed for the electron beam. Nevertheless, electron microscopy has been the main technique for determining the structure of cell organelles, and the obstacles have been partially overcome by, e.g., staining and fixation methods – first chemical fixation and later rapid freezing to avoid ice crystal formation [1]. Selected events in the development of electron microscopy are shown in Table 1.

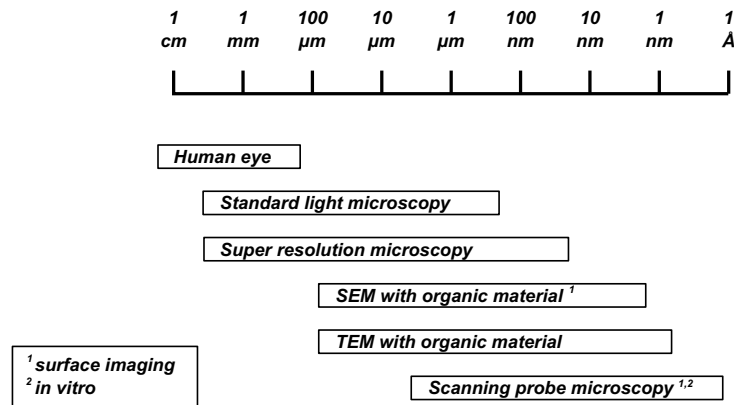


Figure 8: Resolution ranges for different microscopy techniques. Transmission Electron Microscopy (TEM) gives the highest resolution among transmission based microscopy techniques.

Table 1: Selected historical events in the development of modern electron microscopy.

1896	Electrons were focused with a magnetic field by Kristian Birkeland.
1924	Wave theory for electrons developed by Louis Victor de Broglie.
1926	Mathematical foundation of electron optics developed by Hans Busch.
1929-31	The first electron microscope was created by Ernst Ruska and Max Knoll, using the equations developed by Busch.
1958	Manual three-dimensional reconstructions from untilted EM data were presented by Fritiof Sjöstrand and Ebba Cedergren-Andersson.
1968	The first 3-D reconstruction of a macro-molecule was presented by David de Rosier and Aaron Klug.
1984	TEM of adenovirus embedded in vitreous ice.

3.2 Electron microscope

The electron microscope resembles an optical microscope to a high extent. In an optical microscope, the light is focused by the condenser lenses onto the sample and the beam is attenuated by the sample matter, which forms the image pattern that is seen in the microscopic image. This pattern is enlarged by a system of lenses and projected onto a sensor or into an ocular lens for direct viewing. In an electron microscope, the light beam is replaced by a beam of accelerated electrons, and the image is formed by the scattering of beam electrons by the sample matter. Figure 9 shows a conceptual comparison between a light microscope and an electron microscope. The degree of electron scattering correlates with the mass density of the sample. For high density regions in the sample there will be fewer electrons that are transmitted without scattering, which is seen as darker regions in the acquired 2-D image. For 3-D reconstructions, the image intensities are often reversed and high mass densities appear bright and low densities dark.

The electron source in an electron microscope may be similar to the filament in a light bulb – both can be tungsten wires heated to a few thousand degrees. When high voltage is applied to the material, electrons dissipate from it and are accelerated by the high voltage electrical field created by an anode to create the electron beam. However, the best electron sources

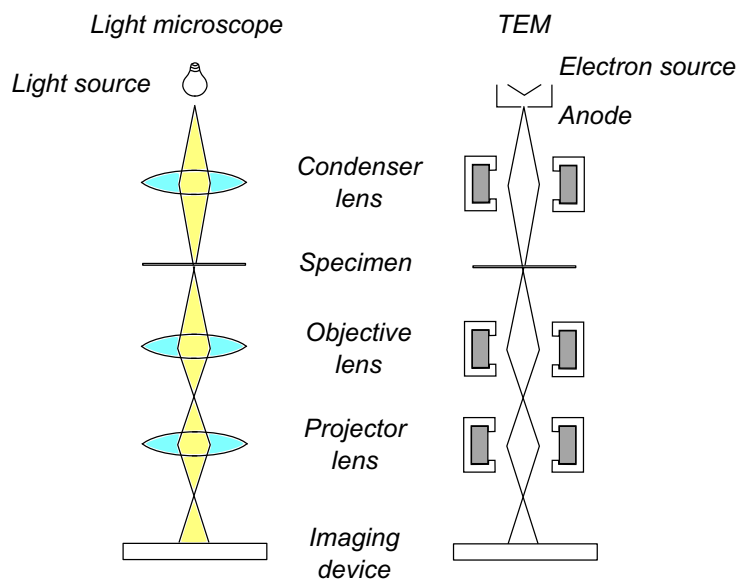


Figure 9: The transmission electron microscope (TEM) shares great similarities with the ordinary light microscope.

are the field emission gun (FEG) filaments. The electrons have less energy variation for field emission guns, and thus the wavelength is more stable. This creates less wavelength dependent aberration (chromatic aberration).

The optics in a light microscope is built on lenses that transform the light beam using the refraction that occurs when light enters and exits the lens material. For electron microscopes, electro-magnetic fields are used to focus and adjust the electron beam. A difficulty is however that charged particles as electrons have a high probability of interacting with other matter. This leads to a considerably higher scattering rate for electrons compared to photons. The standard composition of air would scatter the electrons, and therefore a high quality vacuum is needed inside the microscope. However, organic material cannot be directly exposed to vacuum, as the water inside would evaporate and cause the structure to change too much. The samples need to be fixated, which is performed either chemically or, in cryo-ET, by maintaining cryogenic temperatures using liquid nitrogen. It also is necessary to have thin samples, usually below 200 nm in thickness, for sufficient transmission of the electron beam.

The interaction between the electron beam and sample causes radiation of different kinds, as illustrated in Figure 10. The basis for the image formation is electron beam scattering. This occurs because of Coulomb forces to

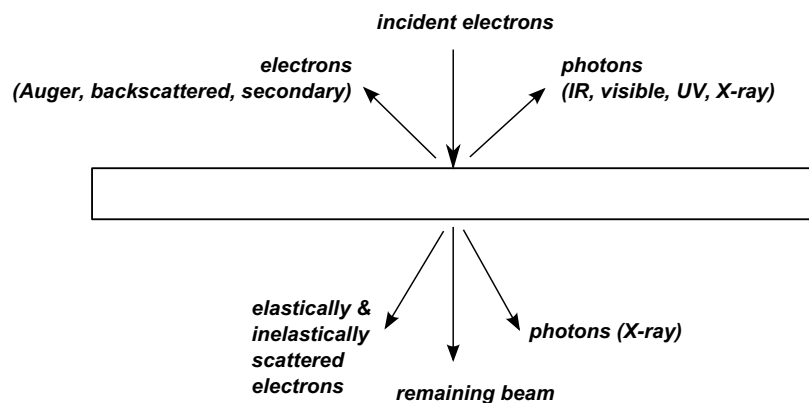


Figure 10: The incident electrons can pass directly through the sample, without interaction, or produce scattered electrons, or transfer part of its energy and produce a photon.

the positively charged nucleus and shell electron, see Figure 11. It can either be *elastic* or *inelastic*. For elastic scattering, the electron preserves its energy, and for inelastic it loses some of it. The electron beam is then projected onto a phosphorous screen or a direct detection sensor, which fairly recently has emerged [34][11]. The phosphorous screen will emit photons where it is hit by electrons. This photon signal is detected by a CCD sensor. After analog to digital conversion, the digital image has been created.

The main noise in a TEM image is *shot noise*, that originates from the small number of electrons hitting each sensor element. If the structure of the material is associated with a certain probability of transmission of an electron, the actual recorded number of electrons may not be a good estimate of the probability, due to the small sampling size.

3.3 Electron tomography

Electron tomography is a subfield of TEM, where the *micrographs*, i.e., the 2-D images from the electron microscope, are combined into a 3-D reconstruction using methods such as filtered back projection (FBP) [22] and iterative refinement (ART [23], SIRT [17], COMET [44]). To achieve this, a *tilt series* of images at different angles is obtained by tilting the sample, usually around one or two axes. For 3-D reconstruction with backprojection, the data from each pixel in every tilt image is smeared out along the projection ray for that pixel, see Figure 12 for a synthetic example. This leads to the intensity at every point in the reconstructed volume being the sum of the smeared out values from the projection rays that pass through that point.

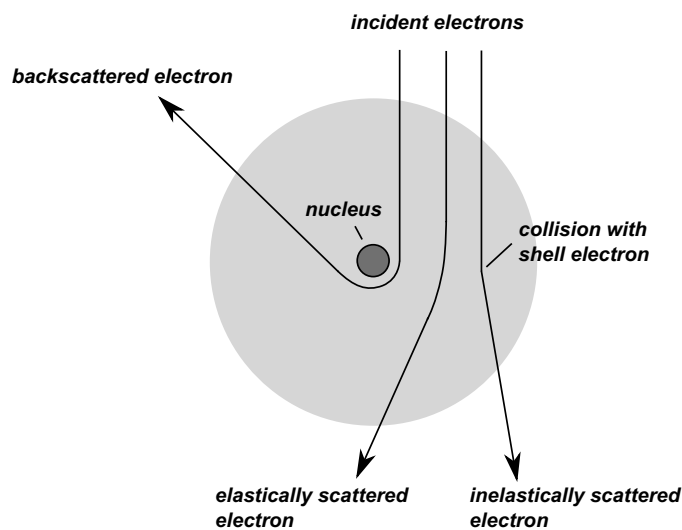


Figure 11: Simplified drawing of scattering events between incident electrons and specimen atoms.

By performing this for all pixels, a basic reconstruction is created that can be used directly, or further enhanced by iterative refinement. The principle behind iterative refinement is to project a reconstructed volume to synthetic tilt images using the point spread function for the used microscope, compare these to the observed tilt images, and correct for the observed deviations by propagating these to the reconstructed volume.

In the first example of 3-D reconstruction published in 1968 [10], only a single image was used. The reconstruction was instead based on the symmetrical properties of the studied object. Symmetry is still much exploited and accounts for when electron microscopy has been used to give the highest resolution reconstructions, of highly symmetrical objects such as viruses.

An important aspect in TEM tomography is the so called *missing data* or *missing angle* problem. It arises due to the fact that the sample can generally only be studied in a limited angular range. When the sample is tilted over 60° , it typically does not give useful reconstruction information. As the sample is tilted, the beam will traverse the sample increasingly diagonally, causing it to travel a longer distance in the sample. Eventually, this will cause too much scattering for the images to be useful. To reduce the problem, the specimen is often tilted around two axes. An interesting new method to get full 180° coverage around one axis, is to encapsulate the material in a lipid nanotube [16]. The tube has a cylindrical shape, and thus the distance the electrons will travel is at maximum the diameter of the tube.

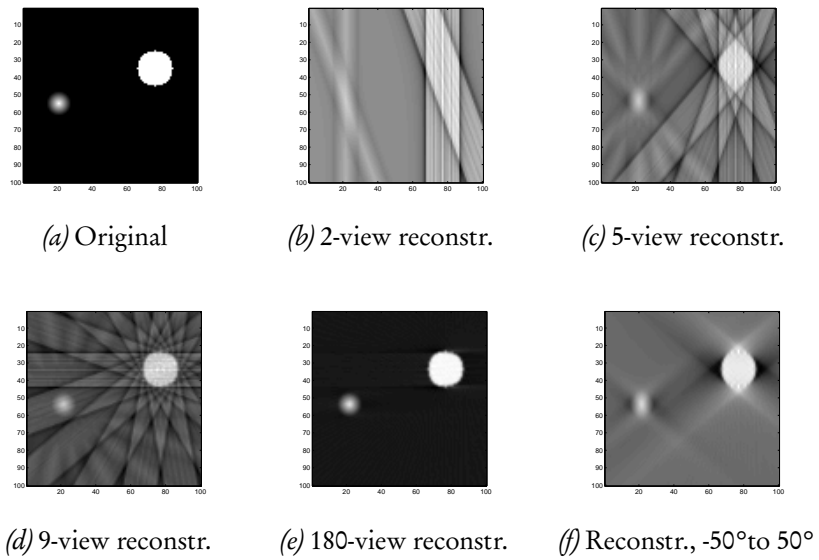


Figure 12: The synthetic 2-D image to the upper-left is reconstructed by backprojection from a different number of views. The views are backprojected along the projection directions. In electron tomography, the reconstruction angle span is not 180° , which can create reconstruction artefacts as in the bottom-right image.

To create a reconstructed volume, it is necessary to find the projection parameters for each view – the images need to be *aligned*. The alignment estimation can be *marker-based* or *markerless*. Different *fiducial markers* can be used, but most common is gold beads of size 10–20 nm. RAPTOR [2] is a software tool for markerless alignment of tilt-series. Requirements for the tilt-series include that, preferably, more than 100 projections should be used, and tilting should be performed in steps 1–2° over a range of at least $\pm 60^\circ$ [5].

Backprojection is a classic reconstruction method that has been used since the field appeared. It is usually combined with ramp filtering in the frequency domain to reduce smearing effects, in a method known as *filtered backprojection* (FBP) [15]. The used ramp filter is passing high frequencies and removes static components, and linearly filters Frequencies. With better computational resources, iterative refinement is now usually added after initial reconstruction by backprojection, based on the techniques described earlier. IMOD [30] is a software for performing reconstructions using iterative refinement. An interesting research area is the regularization used in reconstruction methods. COMET [44] uses entropy based regularization, and recently shape based regularization has appeared [19].

4 Volume visualization and interaction

Computer graphics has evolved much in parallel to computerized image analysis. In computer graphics, visual renderings are generated from mathematical models, whereas in image analysis essentially the reverse is true, i.e., models are generated from images of objects, scenes or samples. The rendering methods in computer graphics are often computationally efficient approximations of light-matter interaction. A first approximation is that light travels along straight lines until it interacts with matter. When light traverse a medium such as a gas or a solid material, different types of physical interaction may occur, primarily

1. reflection or scattering,
2. absorption and transfer of the energy to the material,
3. transmission through it, straight or refracted.

These interactions are simulated in computer graphics, with the aim of rendering realistically looking images with the available computation power. In data visualization, the goal with the rendering is often to bring out specific features of the data or to highlight patterns. The principles for image formation are, however, often the same as when rendering for realistic appearance.

The rendering of volume images can either be performed with direct volume rendering (DVR) [32][12] or indirect volume rendering (IDVR). DVR is based on directly projecting the volume data to a 2-D image, whereas IDVR uses intermediate geometrical representations of the 3-D data, such as polygon models, before projecting it. The geometrical models often represent a subset of the original data, e.g., a particular intensity level, i.e., a *level set*. A surface visualization for distinct intensity levels is denoted an *iso-surface* rendering. In TEM visualization software, iso-surface rendering using IDVR is often the main rendering method. Visualizing a surface using IDVR can in general be computed faster than a DVR because of the reduced, sparse volume representation and because GPUs have been optimized for performing rendering of polygons at high throughput rates for a relatively long time.

DVR is based on direct mapping between 3-D volume data and the 2-D projection. It can be performed by integrating over the viewing rays in a procedure known as *ray casting*. A ray is defined by the viewpoint, field of view and resolution of the rendered image. A conceptual illustration is given in Figure 13. When programmable GPUs was popularized, usage of

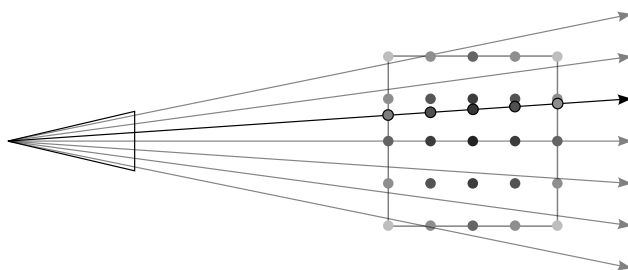


Figure 13: Volume ray casting. Sampling positions are calculated along a straight line from the projection point. Intensities can be accumulated as the line is traversed, according to the opacities of the volume data at the sampling points.

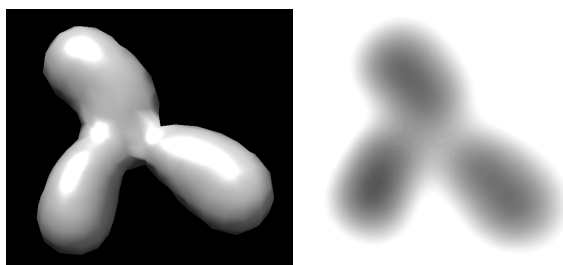


Figure 14: Left: Iso-surface rendering of a density volume with an IgG molecule. The molecular densities are estimated using an atomic model of the molecule, which has been determined using X-ray crystallography. Right: Ray casting visualization of the same molecule.

ray casting increased. First publications on GPU accelerated ray casting appeared in 2003 [40][31]. In Figure 14, an iso-surface visualization, rendered using IDVR, is shown next to a ray casting rendering.

4.1 Ray casting DVR

There are different definitions of the volume rendering integral for ray casting. Here, a definition based on a model with emission and absorption effects is presented. This is an example definition, representing the ray casting model used in this thesis and the physical analogue connected to the model. The volume image is modeled as a collection of particles randomly placed in an open volume. The particles are emissive by glowing with a specific color that is varying in the volume. The particles are furthermore considered non-reflective and opaque, i.e., fully light absorbing. According to this

model, the light intensity changes along a light ray according to

$$\frac{dI}{ds} = c(s) - \tau(s)I(s). \quad (12)$$

where

s	distance from viewpoint along the viewing ray that is cast
$I(s)$	light intensity at distance s
$c(s)$	color emission at distance s
$\tau(s)$	absorption at distance s

In the physical analogy, the emitted light $c(s)$ can be seen as collected along the ray, while the collected light is attenuated by the absorption $\tau(s)$. The solution to this first order differential equation is

$$I(D) = I_0 \exp\left(-\int_0^D \tau(t)dt\right) + \int_0^D c(s) \exp\left(-\int_s^D \tau(t)dt\right) ds, \quad (13)$$

where D is the distance on the ray to integrate over. The first term represents the background color transmitted through the volume and the second term the transmittance of the internal glow. Introducing the transparency $T(s)$ representing

$$T(s) = \exp\left(-\int_s^D \tau(t)dt\right), \quad (14)$$

the equation simplifies to

$$I(D) = I_0 T(0) + \int_0^D c(s) T(s). \quad (15)$$

The integral is calculated numerically as a Riemann sum. To calculate the color emission $c(s)$, the distance along the ray, s , is converted to a 3-D point on the ray by the line defined by the casted ray,

$$f(s) : \mathbb{R} \rightarrow \mathbb{R}^3, \quad (16)$$

$$f(s) = \mathbf{v}s + \mathbf{k}, \quad (17)$$

where \mathbf{v} is the direction of the line and \mathbf{k} a point on the line. At each location $f(s)$ on the ray, the volume is sampled by a function

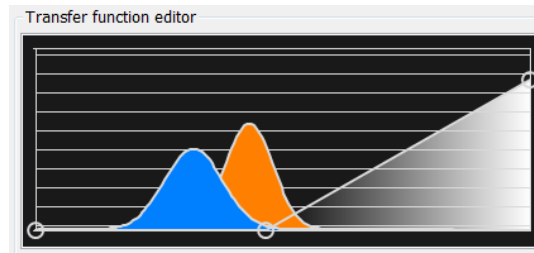


Figure 15: An interactive transfer function editor. The transfer function maps a scalar intensity (x -axis) to a color triplet and an opacity value (y -axis). It is here calculated by summation of the specified transfer function elements. This transfer function include two Gaussian elements (see Paper V), which are not commonly used.

$$v : \mathbb{R}^3 \rightarrow \mathbb{R}. \quad (18)$$

The interpolation is usually linear or cubic, which in the 3-D case is called trilinear or tricubic interpolation. This local estimate of the volume intensity, is translated by the so called *transfer function*,

$$g : \mathbb{R} \rightarrow \mathbb{R}^4, \quad (19)$$

which defines the mapping of a sampled volume value to a color triplet (red, green and blue) and an opacity. The transfer function therefore specifies how the volume data should be colorized and which intensity ranges should be transparent. In practice, it is often specified as a look-up table, defined manually by the user or automatically, according to what should be visualized in the data set. When defined explicitly by the user, it is often setup through a graphical representation of the function, as illustrated in Figure 15.

4.2 Transfer functions and automatic visualization

To ensure that the correct look-up value is used in the transfer function, interpolation should be performed before the transfer function conversion to color and opacity [21]. This is called *post-classification* in contrast to what is denoted *pre-classification*. A related issue is that transfer functions can introduce high frequency components in the signals integrated along the viewing rays, which can lead to alias artefacts [14]. This can be circumvented by supersampling the signal, but this decreases performance. A technique for achieving the same effect, without as large performance reduction, is called

pre-integration, introduced by Engel et al. [14]. In the technique, 2-D look-up tables are pre-calculated to approximate the rendering integral more accurately. Piecewise linear segments are used for calculating the improved approximations of the integral. This has been further improved by the use of second order approximations by El Hajjar et al. [13].

The transfer function is often a direct mapping from the intensities in an image as above, but can also be function of local characteristics as gradient or curvature. Multi-dimensional transfer functions based on curvature was introduced by Kindlmann [28]. Using Gaussians as elements in transfer functions was first suggested by Kniss [29].

An issue with transfer functions is that they are often tedious to set up, and it is hence of interest to automatize transfer function specification [39]. An ideal information basis for defining the transfer function would be a completely identified volume, i.e., the data analysis task would be solved prior to visualization optimization. Approaches from this direction have been denoted *data-centric with model* [39]. However, many automation efforts have concentrated on finding easily computable characteristics, which is denoted *data-centric without model* in the same paper.

Kindlmann has presented semi-automatic transfer function generation that focuses on enhancing boundaries between regions, by studying correlation maps between data value and first and second order derivatives [27]. Bajaj has suggested that properties such as surface area, volume, and gradient integral calculated over the scalar intensity range [3], can be used for transfer function specification. These measures are denoted *contour spectrums*. Rezk Salama has initiated the research of semantically driven transfer function specification, by letting the user interactively set visualization properties for fixed types of tissue material [43].

4.3 Stereoscopic visualization and volume interaction

The standard human-computer interfaces as mouse and trackball devices and ordinary computer screens provide interaction and viewing surfaces in 2-D. Handling of 3-D volume data is possible with these types of devices, but there are 3-D devices that are more natural to use for these types of tasks. Stereoscopic vision techniques have now been popularized in modern TVs. The same technologies can be used to display TEM volume images to benefit from the stereo vision capabilities of human vision. Similarly, the interaction with TEM volume images can also be enhanced with 3-D input devices.

A technology often used in conjunction with stereoscopic vision is *haptics*. It is a technology for letting users feel and touch virtual objects and force field renderings. It has been observed that haptic technology can ben-

efit human performance in certain tasks carried out in 3-D [35]. Research on using haptics for aiding in registration of proteins in TEM images was initiated by Birmanns [7].

5 Contributions

The contributions of this thesis concerns data analysis and visualization of TEM images with a focus on molecular identification. Within this area, a central theme in the research is the use of template matching using static templates and NCC. This is used as a model method, but the contributions in this area (Papers II-IV) are intended to be applicable to different fitting methods and correlation metrics.

5.1 Paper I

In Paper I, it was investigated if a visualization transfer function can be set up automatically for electron tomograms of biological material, using a simplified feature analysis. More specifically, it was studied if histogram and global feature measures can be used to find reference intensity levels, which can be used in the construction of a transfer function, e.g., by defining iso-surface levels.

The standard approach to set visualization parameters manually can be cumbersome and may introduce visualization variability, especially because of the lack of visual cues such as clear borders between components. To perform automatic setup of the visualization transfer function for electron tomograms, suitable reference intensity levels for the visualization need to be established. If the components of the tomogram was already identified, the visualization setup could be based on this identification. However, this is generally not the case, since it is not currently possible to perform automatic identification for the complete tomograms. Hence, a simpler way of extracting information for defining the transfer function is of interest.

It was studied if biological material of interest and noise could be separated in the intensity domain. Five measures were calculated over the intensity range: the ordinary gray-level histogram, a requested connected component measure (the RCC measure), the average gradient, the average curvature, and a weighted average of the other measures. The question posed was if any of the measures, e.g., the gradient or the curvature measures could reveal which intensity levels biomolecules appear at.

To achieve this, the measures was related to a ground truth consisting of user specified intensity levels. An expert user specified parameters to a transfer function with a certain composition. These parameters were directly used as the user specified levels. However, the problem turned out to be challenging and only some correlation between the measures could be found to the primary level, see Figure 16 to see the weighted average level as a function of the expert set level.

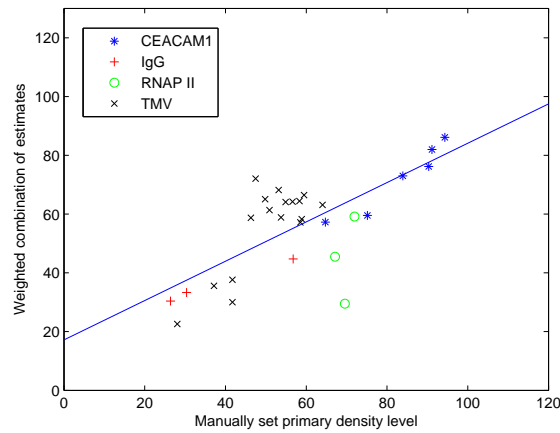


Figure 16: How a weighted combination of the measures correlates to the expert set primary level. The fitted line is used to calculate the performance index of the combined measure.

The RCC measure shows the number of connected components with a specified minimum size, when first thresholding the image at each intensity level. The threshold is increased from the minimum intensity in the image, where all the pixels belong to one connected component. As the threshold is increased, the volume is divided into different connected components, and the RCC measure increase. The components will eventually be smaller than the size limit when the threshold is increased further, and the RCC measure is consequently lowered. The idea with this measure is to see if biological material and noise or artefacts would be maximal at different intensities, giving rise to different peaks in the measure.

For the density histogram, the expert set intensity levels have been translated to histogram percentiles. The distribution was found to be between 95% and 99.8%. Within this range, a correlation to the manual set reference level could be found.

Gradient and curvature measures are calculated at each voxel in the image using the Insight Segmentation and Registration Toolkit (ITK) library⁵. For each bin in the histograms, the gradient and curvature are averaged among the voxels that have intensities covered by that bin, i.e., the set of voxels that are counted in the standard histogram.

⁵<http://www.itk.org/>

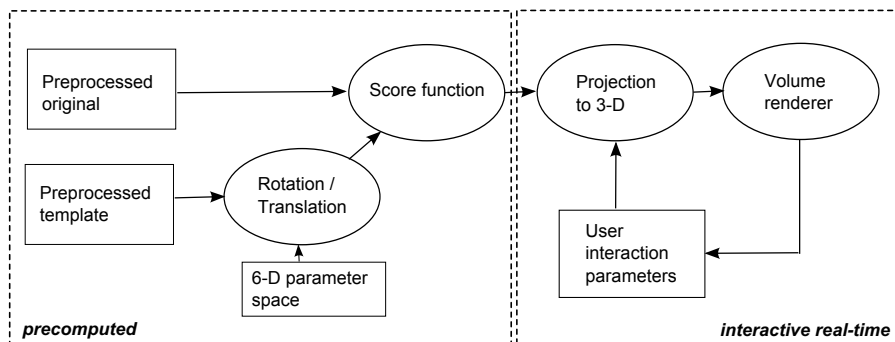


Figure 17: Flowchart for the methodology presented in Paper II.

5.2 Paper II

In Paper II, different techniques for parameter space visualization in relation to template matching are presented. The background issue behind the method is that template matching correlation results may be difficult to interpret and understand. In particular, it is studied how the presented 3-D correlation maps, called scoring volume or score volume, can be visualized using DVR. These scoring volumes can be seen as 3-D fitness landscapes, showing the best matching sites and what rotation of the template gives the highest correlation at those points.

The correlation score between the static template and the searched volume is calculated with NCC for a number of 3-axis rotations at every voxel. This creates a six-dimensional (6-D) correlation space with normalized correlation scores between 0.0 and 1.0. The techniques presented in the paper can be seen as a way of navigating this 6-D space, see Figure 17.

To best see where a template fits, the scoring volume is parametrized over the position parameters (\mathbb{R}^3). The scoring volume will then have the same spatial arrangement as the searched volume, and we opt to visualize them side-by-side. To best see what orientation the template fits at a particular point, the scoring volume is parametrized over the angular space ($SO(3)$) for the template. $SO(n)$ is the special orthogonal group consisting of all orthogonal $n \times n$ matrices that have the determinant 1. $SO(3)$ covers all possible rotations in Euclidean 3-D space.

The intended usage scenario is to run a full correlation search with the correlation metric of choice and be able to interactively explore different matching sites and simultaneously see the corresponding registrations visualizations, as well as graphically seeing how good the fit is in relation to other peaks and the background noise.

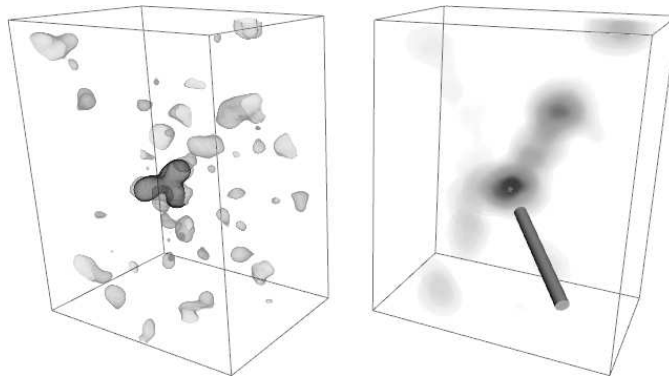


Figure 18: Interactive exploration of an electron tomogram (left) and a *scoring volume* showing the fitness value of the best registration at each position, where the GPU accelerated template matching technique would be an important part of the software.

5.3 Paper III

In Paper III, an evaluation is presented comparing the performance of GPU and CPU implementations of the static template search used in the previous paper. This is a step towards using the template search in an interactive setting in combination with the scoring volume exploration techniques presented in Paper II, see Figure 18. The performance of the correlation search was tested on Nvidia's platform CUDA, on CPU-based Matlab and on Matlab enhanced with the Jacket GPU library⁶, as well as with Colores [9] that provides an optimized CPU based search. The main interest was to study if the GPU acceleration would give speed-ups that enabled interactive use.

CUDA was selected over OpenCL framework, primarily because a 3-D FFT library was available. The implemented pipeline is shown in Figure 19. The data handling and computations of the pipeline are performed on the GPU, after the initial volumes have been transferred to GPU memory. Fourier transformation is used to speed up the calculation, by performing the correlation as a convolution in the Fourier domain. The searched volume is transformed to the Fourier domain once, and the FFT-transformed volume is stored on the GPU throughout the search. The template volume is rotated and FFT-transformed on the GPU, which hence is performed as many times as the number of rotations that should be tested. Rotation is performed using the `tex3d` interpolation call in CUDA with trilinear filtering.

⁶The Jacket library was later incorporated in Matlab.

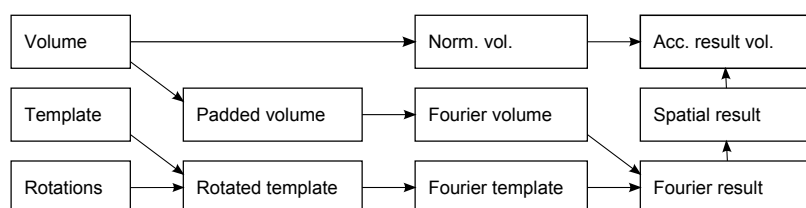


Figure 19: The processing pipeline for the GPU-accelerated template matching. Each box represents one or two memory buffers in CUDA. Memory buffers are reused when possible.

To optimize memory use, buffers are reused in the different steps of the processing. All data is stored in single precision floating point format. The normal padding is determined by the size of the template with the Fourier volume having size (volume size + template size). Additional padding is added to create transformation sizes that are the fastest to compute, at the expense of some memory cost. With well-aligned padding and using CUDA, the performance increases by an order of a magnitude, making it feasible to work with 3-D fitness landscapes, here denoted scoring volumes, that are generated on the fly.

5.4 Paper IV

In Paper IV, a soft probabilistic template (p-template) is introduced, that models molecular flexibility using a static template. The idea is to fix one part of the molecule, and create a volumetric average map for the rest of the molecule or local structure of the molecule. Since the template is static it can be used with a fast correlation routine. This kind of template can be created from either molecular simulation or empirically using observed instances of the molecule, however in this paper only the latter empirical method is explored.

The method is similar to subtomogram averaging, but whereas subtomogram averaging is used to increase resolution, the p-template is used to model flexibility with respect to the alignment points. Another difference is that in subtomogram averaging cross correlation is used to align the subtomograms, where here instead a feature based technique is used.

It is studied how to create such a template for the molecule Immunoglobulin G (IgG). IgG is composed of three parts: one fc-stem and two fab-arms. The two fab-arms are connected to the stem through one hinge region each. This three part system is favorable to model with a p-template using the fc-stem as alignment fixation, since the remaining molecular flexibility does

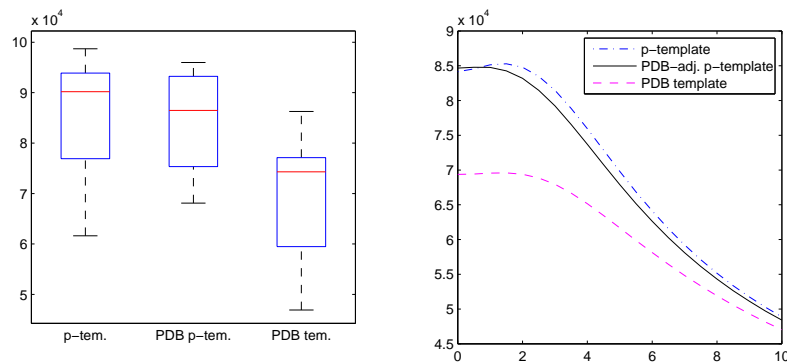


Figure 20: Left: Correlation responses for the standard p-template, PDB-adjusted p-template and PDB template, respectively. The standard p-template performs the best. Right: Average correlation response when increasing the kernel size (sigma) in the Gaussian filtering. The best correlation response is achieved using sigma = 1.5, but the p-template outperforms the PDB-template when using different smoothing as well.

not blur out the fab-arms completely, as far as can be seen using the available IgG instances. It is assumed that the alignment subpart can be approximated as a rigid object, is easily identifiable and can be used to create three alignment points. For the IgG molecule the three reference points are the two hinge regions and the mass center of the fc-stem.

To test the p-templates 12 3-D reconstructed IgG instances are used, with 11 used to construct the template and one used for cross-validation. The data set is small as electron tomograms are difficult to obtain, there is not an abundance of data sets suitable for creating these models. If accurate and reasonably fast molecular simulation was available, the motion range of the molecular components could more easily be established using these. The p-template gives a higher correlation response for the cross-validated test set, see Figure 20.

5.5 Paper V

In Paper V, the software package ProViz is introduced. It presents a tool set for visualization, small particle filtering and template matching, suited for working with electron tomograms. The visualization setup is intended to be easy to use and to give high quality DVR renderings. The small particle filtering removes small connected components, which reduces clutter in the renderings. With the template matching, proteins and other structures can

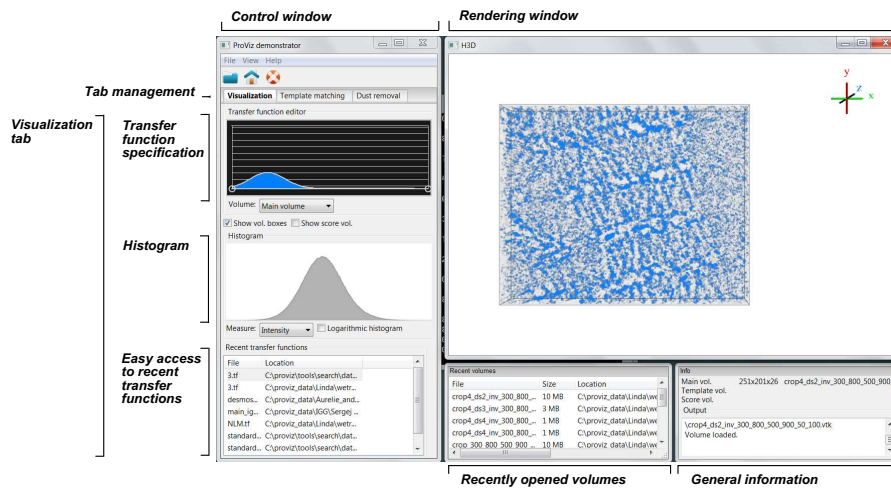


Figure 21: Screenshot of the ProViz program.

be found in the images.

The idea is that ProViz should complement existing software tools as Chimera [38], Sculptor [7] and VMD [25], in particular when working with in situ data and performing template matching analysis. In ProViz it is possible to perform template search and visually assess in ProViz using the GPU acceleration from Paper III and the scoring volume visualization presented in Paper II. The rotational scoring volume is however not included in ProViz. A screenshot of ProViz is shown in Figure 21.

For transfer function specification, a new Gaussian function element is introduced. The Gaussian element is a single color component that can be added and modified similar to a node in the transfer function. The transfer function will consist of a linear sum of the components. Instead of defining the transfer function using nodes, Gaussian elements are used as transfer function building components. This is intended to make it easier to setup a transfer function and also to screen through the intensity range. The visualization settings are automatically stored as the user alters them, and restored when the volume is reloaded.

The software has been developed primarily for Windows, but platform independence has been a consideration. Test versions of the software have been built and run on Ubuntu Linux and on Mac OSX, but these versions are not sufficiently ready to be released publicly.

6 Summary and discussion

A central theme in this thesis is that relatively non-complex image analysis methods have been selected. This approach has been chosen for different reasons: i) because simplicity in itself is often a strength, ii) because of the low SNR of TEM data and iii) because of the lack of training and test data to use for setting parameters in algorithms and models with many degrees of freedom. Concerning the second point, the low SNR of the data increases the importance of retaining useful information during data processing and analysis. Even with intermediate level image analysis methods, such as adaptive filtering, it can be difficult to guarantee that useful information is not lost. Concerning the third point, the lack of annotated training data makes it difficult to create shape based models compared to, e.g., medical image analysis. Manual annotations as ground truth has been avoided, except for in Paper I, where it is only used to set global properties of the visualization.

The presented techniques are focused on improving visualization and template matching in TEM for use in an interactive setting. Specifically, the contributions in the papers are the following.

- In Paper I, it was noted that it is possible to automatically set a reference intensity level based on histogram analysis for TEM tomograms of organic material. For the other measures studied, it was not clear that these provided additional information for automatizing visualization setup, since there were only rather small correlations to the manually specified reference level. The results may be different if the measures were refined, or if reconstructions could be enhanced in terms of spatial resolution or SNR, or if larger data sets were available and used. Automatic transfer function generation has not been studied before for TEM data, to the best of the authors' knowledge.
- In Paper II, explorative visualization and navigation of template matching results in 3-D showed potential, especially when combined with a volume rendering of the TEM data side-by-side. The scoring volume visualization may give a better overview of correlation results and how much the best matching sites stand out in terms of score compared to spurious matches. These types of visualizations might assist a biologist when performing semi-automatic annotations of TEM images or when studying the identification results of automatic volume analysis methods. Similar techniques have been explored by Birmanns and Wriggers [6], which presented the software tools for performing the so called *interactive peak selection* in the *score landscapes* in the same paper. The parameter space exploration methods are related to the

generalized Hough transform [4]. They can be seen as ways of visualizing and navigating multi-dimensional Hough parameter spaces, by projecting these to 3-D subspaces.

- In Paper III, a time performance comparison between different CPU and GPU implementations of template matching was presented. GPU implementations gave, as expected, a large increase in performance, which is important when used interactively. It could also be seen that the performance gap between high level (Matlab JACKET) and medium level (task specific CUDA) GPU programming is still significant. However, GPU programming at medium level was a major undertaking, with especially complicated debugging procedures, despite the development in GPU programming tools in recent years. The software gEMfitter [24] have since been presented for performing GPU accelerated template matching in TEM images.
- In Paper IV, a method for modeling protein flexibility in static templates was presented. The introduced p-template models can be used to model simple molecules with hinge-regions to a central component, or may find use as building blocks when modeling more complex proteins. The p-template creation was demonstrated using subtomogram averaging, but the template could, in theory, also have been created from molecular simulation. While subtomogram averaging aims at increasing resolution, the p-template is aimed at capturing shape variations in the template. With the p-template, static template matching methods can account for object shape variability to a certain extent.
- In Paper V, the software tool ProViz is presented. The tool has been developed during collaboration with biological researchers for visualizing TEM images and for performing explorative template matching (Paper II) with these. One feature, that to the best of the authors' knowledge, does not exist in similar software, is to work with easily modifiable Gaussian components for specifying the transfer function. The ProViz tool is intended to make some of the techniques developed in this thesis available to biologists.

The haptic interface in ProViz is experimental and primarily used for navigation purposes. With the 3-D haptic pen, the interaction with the volume images becomes more similar as to how we use everyday items, which might contribute to a positive user experience by enabling the user to easily and intuitively navigate and select features of interest, but this is a matter for future research.

7 Current development and challenges

There exists a multitude of models and registration methods for molecular analysis of TEM data. TEM data analysis is still often based on registering structures from the Protein Data Bank (PDB) into the tomograms. Recently, matching based on molecular simulation have appeared [45]. Possibly, these kinds of simulations can give reliable statistics on identifications in tomograms in the future.

In a longer time perspective, hypothesis testing in TEM electron tomography may not be a separate post-processing step, but rather incorporated in the microscopy imaging process. If eventually possible, one can imagine that trajectories for individual electrons could be used to test specific reconstruction hypotheses for maximal information gain. In a shorter perspective, regularization may be improved as seen with initial research in shape based regularization [19]. This relates to the interesting question of how to measure information content and density probabilities in a volume. By using accurate molecular models already in the reconstruction, the degrees of freedom estimated during reconstruction would be reduced. This could open possibilities for more accurate reconstructions, which in turn could generate more accurate models. However, with these kinds of reconstruction techniques, accurate validation becomes even more important.

For interactive 3-D tools, there may be great potential in improving how the user interacts with the volumetric data. There are many advanced analysis methods available among the tools developed in the TEM community, but more simple tools, from a user perspective, are perhaps not as readily available.

An idea that I would find interesting to research is that if models with minimum description lengths, e.g., based on spline or wavelet modeling of the data, can be a step in between using molecular model based regularization and existing regularization techniques in TEM tomography. However, this research topic would be in the high risk/high reward category. Other interesting topics include segmentation and identifications performed on a relatively high scale of the data, i.e., on a cellular level rather than on a molecular level. On a higher level, it is easier to establish ground truth data by annotation from biologists.

The processes behind establishing new scientific discoveries often grow more complex, as reaching the next level of insight for a particular research question often requires more elaborate methods. In biological research, test protocols can become longer, more advanced equipment might be needed and the need for data analysis can increase, meaning the number of parameters would increase throughout the whole research process. To balance the

increased complexity, refined research tools are necessary, which, e.g., reduces the number of manual tasks and parameters, and makes the complex processes manageable. The development and research presented in this thesis have aimed at making steps towards this goal.

8 Svensk sammanfattning

Bilddata har fått en alltmer framträdande roll inom forskning och mätteknik. Den digitala utvecklingen har gett möjlighet till större bilddataflöden och samtidigt gjort bildbaserad mätning mer exakt. Dessutom tillkommer specialiserade bildtagningstekniker kontinuerligt, särskilt inom medicinsk bildtagning och inom mikroskopi. En central del i denna digitalisering är utvecklingen inom *digital bildanalys*. Med bildanalys avses i det här sammanhanget att ta fram information ur bilder, t.ex. att hitta objekt i bilderna och att göra bildbaserade mätningar på dessa. I takt med att bilddata har ökat i mängd och blivit mer komplext, har betydelsen även ökat av visualisering och presentation för korrekt bedömning och förståelse av både bilddata och analysresultat. I den här avhandlingen presenteras metoder för bildanalys och visualisering av bilddata från elektronmikroskop av transmissionstyp.

Med elektronmikroskopi är det möjligt att studera organiska strukturer, t.ex. proteiner, på nanometer-nivå. Genom att ta bildserier på ett preparat ur olika vinklar är det möjligt att göra en tre-dimensionell (3-D) rekonstruktion av preparatet, vilket kallas *elektrontomografi*. Rekonstruktionen är i form av en *volymbild*, ett s.k. tomogram, som består av många lager av två-dimensionella (2-D) bilder. Se figur 22 för ett exempel på en 2-D projektion av en sådan volymbild. Bilderna från denna typ av mikroskop är dock svårtolkade. Detta beror bland annat på ett mycket lågt signal-till-brusförhållande, samt att preparatet påverkas och ändrar form både av förbehandlingen av preparatet och av elektronstrålen som används för avbildningen. Avancerad metodik krävs därför för att analysera och ta fram information ur dessa bilder.

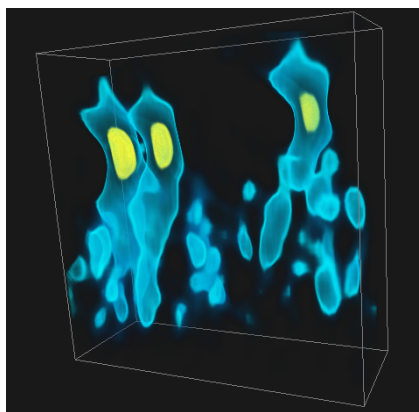


Figure 22: Ett exempel på en projektion av en volymbild på biologiskt material (blått) innehållande antikroppscedjor kopplade till guldpartiklar (gult).

I figur 22 på föregående sida är volymbilden skapad med hjälp av s.k. volymrendering. Visualiseringar av den här typen är ett viktigt verktyg för den utvärdering av bilderna forskare inom biologi gör. Vanligtvis används visualiseringar som är gjorda med iso-yte-rendering eller s.k. raycasting, som är en form direktvolymrendering.

Ett annat verktyg är mönstermatchning av olika typer av molekylmodeller i volymbilderna. Matchningen mellan modellen och den observerade bilden ger ett korrelationsresultat som kan vägleda i bedömningen. Det existerar i dagsläget många sofistikerade molekylära modeller, men det råder en osäkerhet kring vilken valideringsstyrka som uppnås genom att anpassa dessa modeller till bilddata. Modellerna har ofta många frihetsgrader, och det finns forskningsresultat [47] som tyder på att flexibilitetsgraden inte tas tillräckligt väl i beaktande vid tolkning av matchningsresultaten (på grund av att modellerna har så många frihetsgrader kan de också anpassas till alltför många strukturer). Det är av stor betydelse att frihetsgraderna i molekylmodellen också motsvarar molekylens verkliga frihetsgrader.

Det första bidraget i avhandlingen handlar om automatisk visualisering av volymbilder från elektrontomografi. För att visualisera en volymbild behöver parametrar ställas in så att de eftersökta strukturerna syns i renderingen. Artikeln presenterar en undersökning på hur detta kan göras för överföringsfunktionen som definierar hur skalärvärden i volymbilderna ska översättas till färg och opacitet.

Mönstermatchning av volymmodeller i volymbilderna är ett annat område som har studerats. En visualiserings- och navigationsteknik presenteras för utforskning av de korrelationsresultat som mönstermatchningen ger upphov till. Det här ger en ny typ av återkoppling till biologen som tolkar bilden. För att effektivt utnyttja den här visualiseringstekniken, var det önskvärt att hitta ett sätt att förbättra tidsprestandan för mönstermatchningen. Därför undersöktes vidare vilka prestandaförbättringar som kunde uppnås genom utföra beräkningen på en grafikprocessor (GPU) istället. Slutsatsen var att med en GPU-baserad implementation uppnås prestanda som gör att sökning i små volymer går att göra tillräckligt snabbt för att lämpa sig för en interaktiv mjukvara.

Vidare har en alternativ volymmodell för mönstermatchning introducerats. Modellen bygger på att infoga olika formvarianter av proteiner i en volymbild. Det här ger möjlighet till att skapa en densitetskarta som är viktad med sannolikheten för att proteinet täcker en viss voxel. Resultaten visar på att modellen ger högre korrelationsvar på olika konformationer av ett protein än om enbart en statisk molekylmodell används.

Utvalda utvecklade delar har gjorts tillgängliga i en ny mjukvara som

kallas ProViz. Den innehåller interaktiv visualisering av resultat från korrelationssökning, direktvolymrendering i form av raycasting, och volymfiltrering genom bortsortering av små komponenter i volymbilderna. De presenterade metoderna och ProViz-mjukvaran utgör tillsammans ett bidrag till att underlätta för biologerna att utföra forskning med hjälp av elektronmikroskop, genom förbättrade analysmetoder och förenklad hantering av dessa.

References

- [1] M. Adrian, J. Dubochet, J. Lepault, and A. W. McDowell. Cryo-electron microscopy of viruses. *Nature*, 308(5954):32–36, 1984.
- [2] F. Amat, F. Moussavi, L. R. Comolli, G. Elidan, K. H. Downing, and M. Horowitz. Markov random field based automatic image alignment for electron tomography. *Journal of Structural Biology*, 161(3):260–275, 2008.
- [3] C. L. Bajaj, V. Pascucci, and D. R. Schikore. The contour spectrum. In *Proceedings of the 8th Conference on Visualization'97*, pages 167–ff. IEEE Computer Society Press, 1997.
- [4] D. H. Ballard. Generalizing the Hough transform to detect arbitrary shapes. *Pattern Recognition*, 13(2):111–122, 1981.
- [5] K. Batenburg, S. Bals, J. Sijbers, C. Kübel, P. Midgley, J. Hernandez, U. Kaiser, E. Encina, E. Coronado, and G. Van Tendeloo. 3D imaging of nanomaterials by discrete tomography. *Ultramicroscopy*, 109(6):730–740, 2009.
- [6] S. Birmanns, M. Rusu, and W. Wriggers. Using sculptor and situs for simultaneous assembly of atomic components into low-resolution shapes. *Journal of Structural Biology*, 173(3):428 – 435, 2011.
- [7] S. Birmanns and W. Wriggers. Interactive fitting augmented by force-feedback and virtual reality. *Journal of Structural Biology*, 144(1-2):123–131, 2003.
- [8] R. Brunelli. *Template Matching Techniques in Computer Vision: Theory and Practice*. Wiley Publishing, 2009.
- [9] P. Chacón and W. Wriggers. Multi-resolution contour-based fitting of macromolecular structures. *Journal of Molecular Biology*, 317(3):375–384, 2002.
- [10] D. De Rosier and A. Klug. Reconstruction of three dimensional structures from electron micrographs. *Nature*, 217(5124):130–134, 1968.
- [11] G. Deptuch, A. Besson, P. Rehak, M. Szelezniak, J. Wall, M. Winter, and Y. Zhu. Direct electron imaging in electron microscopy with monolithic active pixel sensors. *Ultramicroscopy*, 107(8):674–684, 2007.

- [12] R. A. Drebin, L. Carpenter, and P. Hanrahan. Volume rendering. In *ACM Siggraph Computer Graphics*, volume 22, pages 65–74. ACM, 1988.
- [13] J.-F. El Hajjar, S. Marchesin, J.-M. Dischler, and C. Mongenet. Second order pre-integrated volume rendering. In *IEEE Pacific Visualization Symposium, 2008. Pacific VIS'08.*, pages 9–16. IEEE, 2008.
- [14] K. Engel, M. Kraus, and T. Ertl. High-quality pre-integrated volume rendering using hardware-accelerated pixel shading. In *SIGGRAPH/Eurographics Workshop on Graphics Hardware*, pages 9–16. ACM, 2001.
- [15] J. Frank. *Electron Tomography: Methods for Three-Dimensional Visualization of Structures in the Cell*. Springer, 2006.
- [16] H. Furusho, Y. Mishima, N. Kameta, M. Yamane, M. Masuda, M. Asakawa, I. Yamashita, H. Mori, A. Takaoka, and T. Shimizu. Lipid nanotube encapsulating method in low-energy scanning transmission electron microscopy analyses. *Japanese Journal of Applied Physics*, 48(9):097001, 2009.
- [17] P. Gilbert. Iterative methods for the three-dimensional reconstruction of an object from projections. *Journal of Theoretical Biology*, 36(1):105–117, 1972.
- [18] R. C. Gonzalez and R. E. Woods. *Digital Image Processing (3rd Edition)*. Prentice-Hall, Inc., Upper Saddle River, NJ, USA, 2006.
- [19] A. Gopinath, G. Xu, D. Ress, O. Oktem, S. Subramaniam, and C. Bajaj. Shape-based regularization of electron tomographic reconstruction. *IEEE Transactions on Medical Imaging*, 31(12):2241–2252, 2012.
- [20] I. Grubisic, M. N. Shokhirev, M. Orzechowski, O. Miyashita, and F. Tama. Biased coarse-grained molecular dynamics simulation approach for flexible fitting of X-ray structure into cryo electron microscopy maps. *Journal of Structural Biology*, 169(1):95–105, 2010.
- [21] M. Hadwiger, J. M. Kniss, C. Rezk-salama, D. Weiskopf, and K. Engel. *Real-time Volume Graphics*. A. K. Peters, Ltd., Natick, MA, USA, 2006.
- [22] G. T. Herman. Image reconstruction from projections. *Image Reconstruction from Projections: Implementation and Applications*, 1, 1980.

- [23] G. T. Herman, A. Lent, and S. W. Rowland. ART: mathematics and applications: a report on the mathematical foundations and on the applicability to real data of the algebraic reconstruction techniques. *Journal of Theoretical Biology*, 42(1):1–32, 1973.
- [24] T. V. Hoang, X. Cavin, and D. W. Ritchie. gEMfitter: A highly parallel FFT-based 3D density fitting tool with GPU texture memory acceleration. *Journal of Structural Biology*, 184(2):348–354, 2013.
- [25] W. Humphrey, A. Dalke, and K. Schulten. VMD – Visual Molecular Dynamics. *Journal of Molecular Graphics*, 14:33–38, 1996.
- [26] W. Jiang, M. L. Baker, S. J. Ludtke, and W. Chiu. Bridging the information gap: computational tools for intermediate resolution structure interpretation. *Journal of Molecular Biology*, 308(5):1033–1044, 2001.
- [27] G. Kindlmann and J. W. Durkin. Semi-automatic generation of transfer functions for direct volume rendering. In *Proceedings of the 1998 IEEE Symposium on Volume Visualization*, pages 79–86. ACM, 1998.
- [28] G. Kindlmann, R. Whitaker, T. Tasdizen, and T. Moller. Curvature-based transfer functions for direct volume rendering: Methods and applications. In *Proceedings of the 14th IEEE Visualization 2003 (VIS'03)*, pages 513–520. IEEE, 2003.
- [29] J. Kniss, S. Premoze, M. Ikits, A. Lefohn, C. Hansen, and E. Praun. Gaussian transfer functions for multi-field volume visualization. In *Proceedings of the 14th IEEE Visualization 2003 (VIS'03)*, pages 497–504. IEEE, 2003.
- [30] J. R. Kremer, D. N. Mastrorarde, and J. McIntosh. Computer visualization of three-dimensional image data using imod. *Journal of Structural Biology*, 116(1):71 – 76, 1996.
- [31] J. Kruger and R. Westermann. Acceleration techniques for gpu-based volume rendering. In *Proceedings of the 14th IEEE Visualization 2003 (VIS'03)*, page 38. IEEE Computer Society, 2003.
- [32] M. Levoy. Display of surfaces from volume data. *IEEE Computer Graphics and Applications*, 8(3):29–37, 1988.
- [33] J. P. Lewis. Fast normalized cross-correlation. *Vision Interface*, 10(1):120–123, 1995.

- [34] A.-C. Milazzo, P. Leblanc, F. Duttweiler, L. Jin, J. C. Bouwer, S. Peltier, M. Ellisman, F. Bieser, H. S. Matis, H. Wieman, P. Denes, S. Kleinfelder, and N.-H. Xuong. Active pixel sensor array as a detector for electron microscopy. *Ultramicroscopy*, 104(2):152 – 159, 2005.
- [35] O.-Y. Ming, D. V. Beard, and F. Brooks. Force display performs better than visual display in a simple 6-d docking task. In *Proceedings of 1989 IEEE International Conference on Robotics and Automation*, pages 1462–1466. IEEE, 1989.
- [36] S. Nickell, C. Kofler, A. P. Leis, and W. Baumeister. A visual approach to proteomics. *Nature Reviews Molecular Cell Biology*, 7(3):225–230, 2006.
- [37] M. Orzechowski and F. Tama. Flexible fitting of high-resolution X-ray structures into cryoelectron microscopy maps using biased molecular dynamics simulations. *Biophysical Journal*, 95(12):5692–5705, 2008.
- [38] E. F. Pettersen, T. D. Goddard, C. C. Huang, G. S. Couch, D. M. Greenblatt, E. C. Meng, and T. E. Ferrin. UCSF Chimera - a visualization system for exploratory research and analysis. *Journal of Computational Chemistry*, 25(13):1605–1612, 2004.
- [39] H. Pfister, B. Lorenzen, C. Bajaj, G. Kindlmann, W. Schroeder, L. S. Avila, K. Raghu, R. Machiraju, and J. Lee. The transfer function bake-off. *IEEE Computer Graphics and Applications*, 21(3):16–22, 2001.
- [40] S. Roettger, S. Guthe, D. Weiskopf, T. Ertl, and W. Strasser. Smart hardware-accelerated volume rendering. In *Proceedings of the symposium on Data visualisation 2003 (VISSYM '03)*, volume 3, pages 231–238. Citeseer, 2003.
- [41] A. M. Roseman. Docking structures of domains into maps from cryoelectron microscopy using local correlation. *Acta Crystallographica Section D: Biological Crystallography*, 56(10):1332–1340, 2000.
- [42] M. G. Rossmann. Fitting atomic models into electron-microscopy maps. *Acta Crystallographica Section D: Biological Crystallography*, 56(10):1341–1349, 2000.
- [43] C. R. Salama, M. Keller, and P. Kohlmann. High-level user interfaces for transfer function design with semantics. *IEEE Transactions on Visualization and Computer Graphics*, 12(5):1021–1028, 2006.

- [44] U. Skoglund, L.-G. Öfverstedt, R. M. Burnett, and G. Bricogne. Maximum-entropy three-dimensional reconstruction with deconvolution of the contrast transfer function: A test application with adenovirus. *Journal of Structural Biology*, 117:173–188, 1996.
- [45] L. G. Trabuco, E. Villa, K. Mitra, J. Frank, and K. Schulten. Flexible fitting of atomic structures into electron microscopy maps using molecular dynamics. *Structure*, 16(5):673 – 683, 2008.
- [46] D. Vasishtan and M. Topf. Scoring functions for cryoEM density fitting. *Journal of Structural Biology*, 174(2):333–343, 2011.
- [47] N. Volkman. Confidence intervals for fitting of atomic models into low-resolution densities. *Acta Crystallographica Section D: Biological Crystallography*, 65(7):679–689, 2009.
- [48] N. Volkman and D. Hanein. Quantitative fitting of atomic models into observed densities derived by electron microscopy. *Journal of Structural Biology*, 125(2):176–184, 1999.
- [49] W. Wriggers and P. Chacon. Modeling tricks and fitting techniques for multi-resolution structures. *Structure*, 9:779 – 788, 2001.
- [50] W. Wriggers, R. A. Milligan, and J. A. McCammon. Situs: a package for docking crystal structures into low-resolution maps from electron microscopy. *Journal of Structural Biology*, 125(2):185–195, 1999.
- [51] W. Wriggers, Z. Zhang, M. Shah, and D. C. Sorensen. Simulating nanoscale functional motions of biomolecules. *Molecular Simulation*, 32(10-11):803–815, 2006.
- [52] Z. Yang, K. Lasker, D. Schneidman-Duhovny, B. Webb, C. C. Huang, E. F. Pettersen, T. D. Goddard, E. C. Meng, A. Sali, and T. E. Ferrin. UCSF Chimera, MODELLER, and IMP: An integrated modeling system. *Journal of Structural Biology*, 179(3):269–278, 2012.

Acknowledgements

First, I thank the Swedish University of Agricultural Sciences and Uppsala University where this work has been carried out, as well as the funding agencies supporting the ProViz project: the Knowledge Foundation, Vårdal Foundation, the Foundation for Strategic Research, VINNOVA, and Invest in Sweden Agency. I also want to thank everyone that has helped along the journey in one way or another, especially the CBA/Vi2 department for discussions, feedback, ideas and team spirit. Special thanks go to the following people:

- Ida-Maria Sintorn, my main supervisor, thanks very much for the good guidance in the research and academic world, for the big support and encouragement and for good advice that holds long beyond the PhD studies. An extra thanks for the contribution in making the research visit to OIST in Okinawa possible.
- Stina Svensson, my first main supervisor, for pursuing the grant that initiated the ProViz project, for selecting me for the PhD position, for good guidance, sensible advice and much encouragement during the early time, especially in introducing me to analysis in electron microscopy.
- Ingela Nyström, my assistant supervisor, for your part in the initialization of the ProViz project, for good guidance, for bringing new viewpoints into my consideration and thanks for the feedback on my texts.
- Gunilla Borgefors, my supervisor, for good advice and encouragement, for giving me well-needed space and for bringing calmness to the research atmosphere during the weekly meetings.
- Anders Brun, for sharing good ideas and advice, for recommending interesting papers and for the active contribution regarding the development of the explorative template matching technique.
- Fredrik Nysjö, Johan Nysjö and Daniel Evestedt, for your contributions to the ProViz software, for insightful discussions and for sharing your extensive knowledge about software libraries and frameworks. An extra thanks to Johan for nice cooperation in course labs and to Fredrik for the collaboration during the past year.
- Huy Nguyen, for the contribution to the ProViz software, and for great Skype cooperation although we never met (yet) IRL.

- Aurelie Laloef, Lianne den Hollander, Linda Sandblad, Sergej Masich and Lars Norlén at Karolinska Institutet and Umeå University, for sharing your data, for taking the time to explain the biological research questions, for valuable discussions, ideas and feedback.
- Ulf Skoglund, for giving me the possibility to visit OIST in Okinawa for two months and learn a lot. Thanks to Lars-Göran Öfverstedt, Hirotoshi Furusho and Jakub Kolodziejczyk for discussions during the visit and for being so nice and friendly. Visiting OIST and Okinawa was truly a spectacular experience ☺
- Lena Nordström, for all the help with administration and for reminding me about important things.
- Shizuka Kuda, for all the help to go through the administration related to visiting OIST, and for the help during the visit.
- Olle Eriksson, for mentoring in teaching and for providing a good computer environment.
- Maria Israelsson Nordström at SLU Umeå, for the general support.
- Cris Luengo, for sharing your knowledge.
- Ewert Bengtsson, for positive feedback and for the respectfulness and nice tone towards everyone in discussions.
- Hamid Sarve, for good mentorship (fadderskap).
- Maria Axelsson, for interesting discussions.
- Bettina Selig, for sharing valuable experiences, for supporting a good atmosphere at the office and for friendship.
- Vladimir Curic, for interesting discussions, for friendship and for the tip about the JSPS-grant that made the OIST visit possible.
- Jens Hedrich, for interesting discussions and friendship.
- Azadeh Fakhrzadeh, for good advice and for cheerful friendship.
- Omer Ishaq, for interesting discussions and for sharing good advice.
- My friends Bobby Almroth & Josephine Betschart, Andreas Edlund, Daniel Aurell, Mikael Aurell, Erik Stenborg & Yoko Kumagai, Jan Mårts and Robert Ljung, for learning very much from you and for

fun and inspiring times, although too seldom. Sorry for not being good at keeping up contact during these years.

- まさしさん、かつえさんへ わたし が しごと で
にほんへ いくたび いつも わたし を サポート
してくださって ありがとうございます。
- My family Monica, Bert and Jürgen for the great support in all kinds of situations. Sorry for my limited availability during the PhD studies.
- Midori, for your love, for making me happy and relaxed, for always being on my side, for reminding me to take it easy and rest, for oishii food ☺ ありがとうございます。 I love you very much ♡